Neurobiology of Aging 100 (2021) 59–71

Contents lists available at ScienceDirect

Neurobiology of Aging

journal homepage: www.elsevier.com/locate/neuaging

Complex and regional-specific changes in the morphological complexity of GFAP$^+$ astrocytes in middle-aged mice

Heather Bondi[a,b], Valeria Bortolotto[a,b], Pier Luigi Canonico[b], Mariagrazia Grilli[a,b,*]

[a] Laboratory of Neuroplasticity, Department of Pharmaceutical Sciences, University of Piemonte Orientale, Novara, Italy
[b] Department of Pharmaceutical Sciences, University of Piemonte Orientale, Novara, Italy

ARTICLE INFO

Article history:
Received 21 September 2020
Received in revised form 14 December 2020
Accepted 19 December 2020
Available online 30 December 2020

Keywords:
Astrocyte
Aging
Dorsal hippocampus
Dentate gyrus
Morphometry
Neurogenesis

ABSTRACT

During aging, alterations in astrocyte phenotype occur in areas associated with age-related cognitive decline, including hippocampus. Previous work reported subregion-specific changes in surface, volume, and soma size of hippocampal astrocytes during physiological aging. Herein we extensively analyzed, by morphometric analysis, fine morphological features of GFAP$^+$ astrocytes in young (6-month-old) and middle-aged (14-month-old) male mice. We observed remarkable heterogeneity in the astrocytic response to aging in distinct subfields and along the dorsoventral axis of hippocampus and in entorhinal cortex. In middle-aged mice dorsal granule cell and molecular layers, but not hilus, astrocytes underwent remarkable increase in their morphological complexity. These changes were absent in ventral Dentate Gyrus (DG). In addition, in entorhinal cortex, the major input to dorsal DG, astrocytes underwent remarkable atrophic changes in middle-aged mice. Since dorsal DG, and not ventral DG, is involved in cognitive functions, these findings appear worth of further evaluation. Our findings also suggest an additional level of complexity in the structural changes associated with brain aging.

1. Introduction

With physiological aging, cognitive decline can manifest as deficits in specific tasks, including attention, spatial learning, episodic memory, and working memory (Bettio et al., 2017; Dahan et al., 2020). Decades of intense research activities have correlated age-related impairment in cognitive functions to anatomical, cellular, and molecular alterations occurring in vulnerable brain regions and subfields. The hippocampus appears to be particularly vulnerable to the aging process (Geinisman et al., 1995; Mota et al., 2019). For example, both in humans and animal models, loss of functional synapses in cornu ammonis 1 (CA1) and dentate gyrus (DG) (Burger, 2010; Rosenzweig and Barnes, 2003) has been extensively described in response to aging. Moreover, aging is associated with impairment of adult hippocampal neurogenesis (ahNG), a peculiar form of neuroplasticity which contributes to cognition (Bettio et al., 2017; Lazarov et al., 2010; Seib and Martin-Villalba, 2015). Interestingly, dorsal hippocampus (dHp), and not ventral hippocampus (vHp), has been more closely connected with cognitive functions (Fanselow and Dong, 2010). Similarly, modulation of ahNG in the dHp is more correlated with cognitive performance (Strange et al., 2014; Tanti and Belzung, 2013).

In the past, most age-related studies have focused on functional changes in neural networks and/or alterations in neuronal morphology, whereas aging effects on glial cells have remained largely overlooked. In the central nervous system (CNS) astrocytes perform key roles in normal brain physiology, providing trophic support to neurons, participating in synaptic function and plasticity, mediating uptake and recycling of neurotransmitters and maintaining of the blood–brain barrier (Augusto-Oliveira et al., 2020; Verkhratsky et al., 2019, 2020; Verkhratsky and Nedergaard, 2018). In addition, in the DG astrocytes actively modulate the differentiation, growth, survival, and integration of adult born neuroblasts and neurons via both cell to cell contact and release of soluble molecules (Cassé et al., 2018; Cvijetic et al., 2017; Spampinato et al., 2019). In human as well as in rodent brain, alterations in astrocytes phenotype occur with aging (Matias et al., 2019; Verkhratsky et al., 2019). These morphological changes are mainly observed in specific brain areas associated with age-related cognitive decline, including the hippocampus (Palmer and Ousman, 2018). Subregion-specific responses of hippocampal astrocytes in terms of surface, volume, and soma size during aging have also been reported (Rodríguez et al., 2014).

* Corresponding author at: Department of Pharmaceutical Sciences, University of Piemonte Orientale, Via Bovio 6, 28100 Novara, Italy. Tel.: +39 321 375828; fax: +39-0321375621.
E-mail address: mariagrazia.grilli@uniupo.it (M. Grilli).

0197-4580/
https://doi.org/10.1016/j.neurobiolaging.2020.12.018

Herein we decided to extend current knowledge about fine morphological changes occurring in astrocytes during physiological brain aging. In particular, we performed morphometric analysis of glial fibrillary acidic protein (GFAP) immunolabeled astrocytes in young (6-month-old [6-mo]) and middle-aged (14-month-old [14-mo]) male mice. We focused our attention on brain areas associated with age-related cognitive decline, namely the DG subfields Granule Cell Layer (GCL), molecular layer (ML), hilus (H), the CA1 stratum Lacunosum Moleculare (sLM), and the entorhinal cortex (EC). Based on the anatomical and functional organization of hippocampus along the dorsoventral axis (Fanselow and Dong, 2010), we also evaluated age effects on astrocyte morphology in the dorsal and ventral DG.

2. Materials and methods

2.1. Animals

Adult male C57BL/6J mice of 2 different ages (6-mo, $n = 4$; 14-mo, $n = 5$) were utilized. Mice, kept 3–4/cage with access to water and food ad libitum, were housed in a light- and temperature-controlled room in high-efficiency particulate air–filtered Thoren units (Thoren Caging Systems) at the University of Piemonte Orientale animal facility. Animal care and handling were performed in accordance with the Italian law on animal care (D.L. 26/2014), as well as European Directive (2010/63/UE) and approved by the Organismo Preposto al Benessere Animale of University of Piemonte Orientale, Novara, Italy.

2.2. Tissue preparation

Mice were deeply anesthetized and transcardially perfused with saline solution and then with 4% paraformaldehyde (PFA) in 0.1 M phosphate buffer, pH 7.4. After PFA perfusion, brains were rapidly removed, post-fixed in PFA for 24 hours, dehydrated in 15% sucrose for 24 hours, and then transferred in sucrose 30% for at least 24 hours. Then, 40-μm-thick coronal sections were cut with cryostat and collected in cryoprotectant solution at −20 °C until use.

2.3. Immunohistochemistry and image acquisition

The different brain areas included in the analysis were delineated according to the Paxinos Mouse Brain Atlas (Paxinos and Franklin, 2004). From a complete series of one-in 8 brain sections throughout the entire DG, 3 corresponding sections were selected from Bregma −0.94 to −2.46 (dHp) for analysis of astrocytes in the sLM, ML, GCL, and H. For astrocytes in the lateral EC, 4 corresponding sections/mouse located from Bregma −2.54 to −4.04 mm were analyzed. Staining was performed on free floating sections. Endogenous peroxidase activity was blocked with 0.3% H_2O_2 in 0.1 M tris-buffered saline (TBS) for 10 minutes. Sections were subsequently treated at 4 °C for 1 hour in a blocking solution containing 10% horse serum (HS), 0.3% Triton X-100 in 0.1 M TBS, pH 7.4, and incubated with goat polyclonal anti-GFAP antibody (cod. SC-6170, 1:100; Santa Cruz Biotechnology) in 2% HS, 0.1% Triton X-100 in 0.1 M TBS, overnight at 4 °C. Then, sections were incubated with biotinylated horse anti-goat secondary antibody (cod. BA-9500, 1:200; Vector Laboratories) in 2% HS in 0.1 M TBS for 1.5 hours at 4 °C. Labeled cells were visualized using the ABC system (cod. PK-6100, Vectastain Elite; Vector Laboratories) with 3,3′-diaminobenzidine as chromogen (cod. D3939; Sigma-Aldrich), and nuclei were counterstained with hematoxylin (cod. H3404; Vector Laboratories). Images were acquired using an LSM700 laser-scanning confocal microscope (Carl Zeiss, Le Pecq, France) with 20× magnification (objective: EC Plan-Neofluar 20×/0.5 M27) with an image matrix of 1024 × 1024 pixel, a pixel scaling of 0.313 × 0.313 μm, and a depth of 8 bit. Confocal images were collected in Z-stacks with a slice distance of 0.4 μm.

2.4. Three-dimensional astrocyte reconstruction and quantitative morphometry

The image stacks were imported into FIJI software (version 1.52), where three-dimensional (3D) reconstructions were performed with the Simple Neurite Tracer plugin (Longair et al., 2011) by an investigator blinded to animal group. Only astrocytes that exhibited fully intact GFAP-immunostained processes were chosen for reconstruction ($n = 12$ astrocytes per animal, per region). In the GCL, cell tracing was restricted to astrocytes with the soma located in the outer or middle third of GCL to incidentally avoid inclusion of radial glia cells located in the inner GCL and subgranular zone. Morphological analysis was performed on 3D reconstructions of astrocytes by the Sholl analysis plugin (Ferreira et al., 2014), using default settings (enclosing radius cutoff = 1 intersection, Sholl method = linear) with radii increasing by 5 μm. The Sholl intersection profile (SIP) counts the number of intersections between astrocytic process and concentric spheres emanating from the center of cell soma. Some morphometric descriptors have been also included in our analysis (i.e., total number of intersections and radius of highest count of intersections). Moreover, 3D reconstructions were exported as SWC files and analyzed with L-measure tool to evaluate additional morphometric features such as number of processes, total length and maximum process extension (Scorcioni et al., 2008).

2.5. Statistical analysis

All statistical analyses and data visualizations were performed in RStudio version 1.2.5 (RStudio Team, 2015) using R version 3.5.1 (R Core Team, 2016) and the packages ggplot2 (Wickham, 2016), dplyr (Wickham et al., 2018), lme4 (Bates et al., 2015), and multcomp (Hothorn et al., 2008). For statistical analysis of morphological parameters, a linear mixed-effects model was used to model the data of each parameter, with age as fixed effects and animal as a random effect (with lmer package). Using this approach, it is possible to overcome the dependency of the repeated observations within each animal (Bortolotto et al., 2019). The presence of significant differences was tested using one-way analysis of variance. SIPs were analyzed by mixed-effects nested analysis of variance approach with individual animal as random effect and radius nested within astrocytes nested within age. Statistical analysis of morphological differences between brain areas within each age group was performed using mixed-effect models with post hoc Tukey's honestly significant difference (HSD) correction (using multcomp package). For all analyses, significance was defined as $p < 0.05$. Data are presented as mean ± standard deviation.

3. Results

In order to investigate potential hippocampal subregion-specific changes in astrocyte morphology during physiological aging, we profiled cells from 6-mo and 14-mo C57BL/6J male mice in the following subfields: GCL, ML, H, and sLM. Initially, we focused our analysis on the dHp, since this region is more related to cognition (Fanselow and Dong, 2010; Strange et al., 2014).

3.1. Astrocytes in the dGCL show an age-related increase in their morphological complexity

First, we examined astrocytes in the dorsal Granule Cell Layer (dGCL) (Fig. 1A). In this subfield, cell tracing was restricted to astrocytes with their soma located in the outer or middle third of dGCL to incidentally avoid the possibility of including $GFAP^+$ radial glia cells which are located in the inner dGCL and subgranular zone. By Sholl analysis it is possible to resolve on a one-dimensional representation (SIP) the complexity of the 3D astrocyte structure in both 6-mo and 14-mo mice. Astrocytes from 14-mo mice displayed increased complexity of process arborization at 10–25 μm distances from the soma, when compared to younger mice (Fig. 1B). Moreover, we observed a statistically significant increase in the sum of intersections in 14-mo compared to 6-mo mice (4-mo: 62.55 ± 17.16 μm, 6-mo: 49.42 ± 16.84 μm, $p = 0.005$; Fig. 1C). Further analysis of 3D reconstructions by L-measure tool allowed to evaluate additional morphometric features such as number of processes, total length, and maximum process extension. At middle age, compared to younger mice, dGCL astrocytes showed an increase in the total process length (4-mo: 428.27 ± 115.54 μm, 6-mo: 322.96 ± 112.69 μm, $p = 0.003$; Fig. 1C) and in the number of processes (4-mo: 21.80 ± 5.17, 6-mo: 16.83 ± 5.22, $p = 0.002$; Fig. 1C). Despite the increased complexity, processes of astrocytes of 14-mo mice extended to distances similar to 6-mo group (Fig. 1C).

3.2. In the dorsal molecular layer of middle-aged mice, astrocytes have increased morphological complexity

Astrocytes in the dorsal Molecular Layer (dML) were also analyzed (Fig. 2A). Our morphological analysis demonstrated that, in this brain area, astrocytes from 14-mo mice showed a more complex arborization than those of 6-mo animals. Specifically, the analysis of SIP indicated an increase of complexity between 5 and 40 μm from somata in 14-mo compared to 6-mo mice (Fig. 2B). Total number of intersections was also increased with age (14-mo: 57.68 ± 13.98, 6-mo: 38.85 ± 10.47, $p = 0.002$; Fig. 2C). Higher complexity of astrocytes in 14-mo animals was also underlined by the increase in the total process length (14-mo: 382.78 ± 87.38 μm, 6-mo: 255.21 ± 68.48 μm, $p = 0.001$; Fig. 2C), in the number of processes (14-mo: 21.60 ± 5.47, 6-mo: 15.08 ± 4.42, $p = 0.008$;

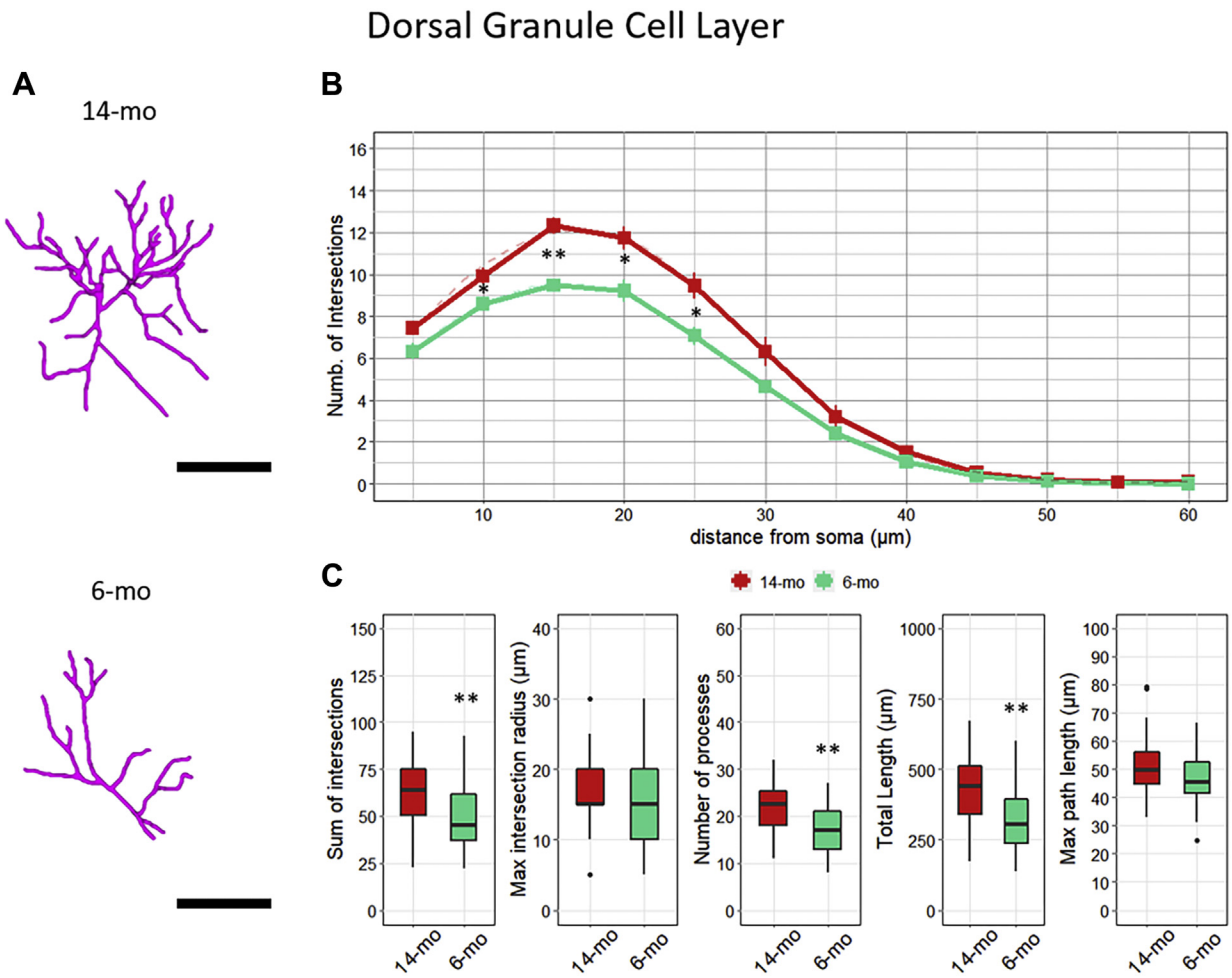

Fig. 1. Astrocytes in the dGCL show an age-related increase in their morphological complexity. (A) Representative 3D morphological reconstruction of astrocyte in the dGCL of 14-mo (upper panel) and 6-mo (lower panel) mice, scale bar: 25 μm. (B) Sholl intersection profiles show that astrocytic morphological complexity in dGCL was significantly increased in 14-mo (red) versus 6-mo (green) mice. Data are presented as mean ± SEM. * $p < 0.05$, ** $p < 0.01$; nested ANOVA on linear mixed-effect model, with animal as a random effect. (C) Summary of morphometric parameters illustrating the total number of intersections, the distance from the somata with the higher number of intersections, the number of astrocytic processes, total processes length, and the maximum reached extension. In each box plot, the heavy line represents the sample median, the box demarks the range from 25% to 75% of the data, limits of vertical lines (whiskers) represent the min and max values, excluding outliers (dots). ** $p < 0.01$; ANOVA on linear mixed-effect model, with animal as a random effect. Abbreviations: 3D, three-dimensional; 6-mo, 6-month-old; 14-mo, 14-month-old; ANOVA, analysis of variance; dGCL, dorsal Granule Cell Layer; SEM, standard error of the mean. (For interpretation of the references to color in this figure legend, the reader is referred to the Web version of this article.)

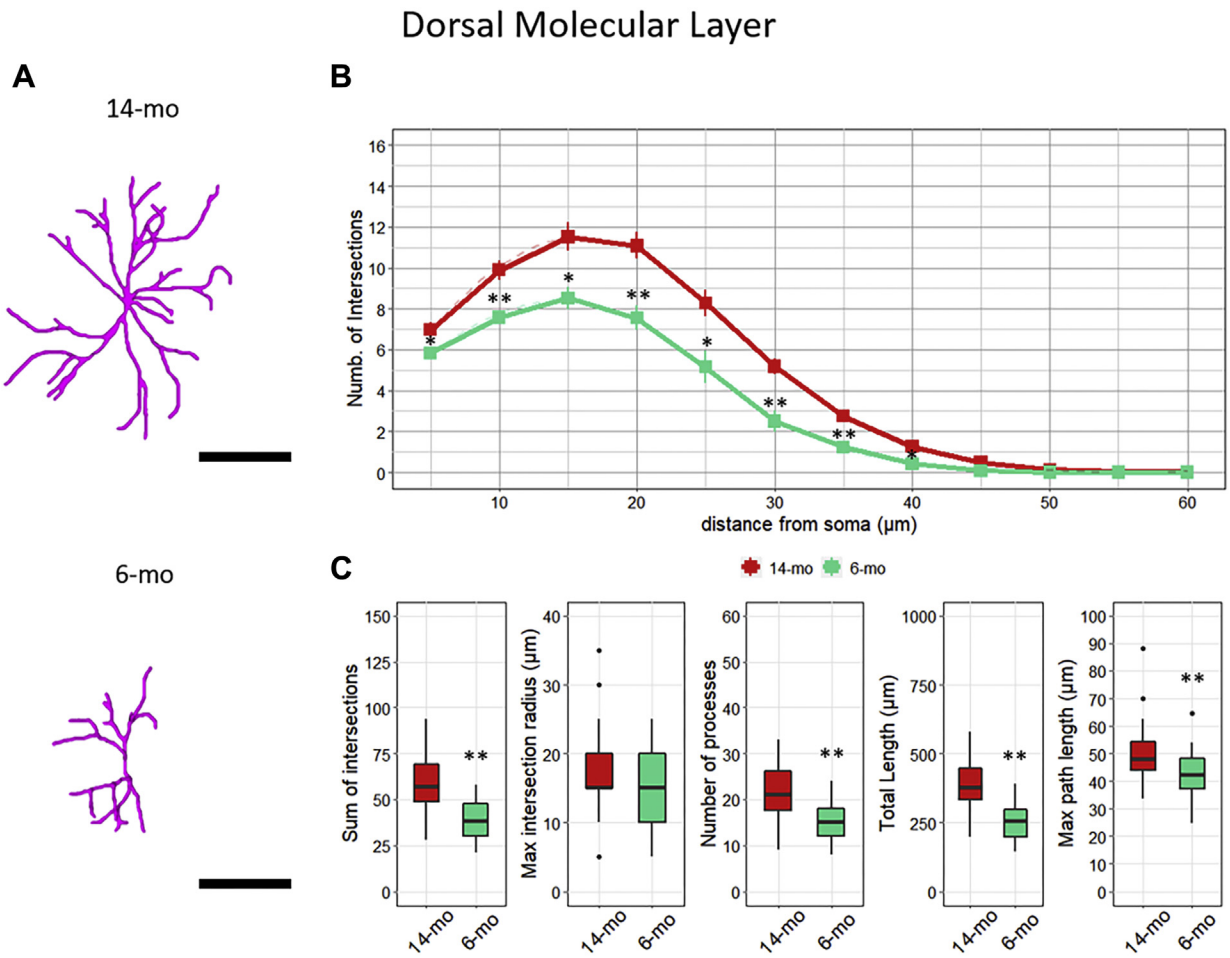

Fig. 2. Increase in morphological complexity of astrocytes in the dML of middle-aged mice. (A) Representative 3D morphological reconstruction of astrocyte in the dML of 14-mo (upper panel) and 6-mo (lower panel) mice, scale bar: 25 µm. (B) Sholl intersection profiles show that astrocytic complexity in the dML was significantly increased in 14-mo (red) versus 16-mo (green) mice. Data are presented as mean ± SEM. * $p < 0.05$, ** $p < 0.01$; nested ANOVA on linear mixed-effect model with animal as a random effect. (C) Summary of morphometric parameters illustrating the total number of intersections, the distance from the somata with the higher number of intersections, the number of astrocytic processes, total processes length, and the maximum reached extension. In each box plot, the heavy line represents the sample median, the box demarks the range from 25% to 75% of the data, limits of vertical lines (whiskers) represent the minimum and maximum values, excluding outliers (dots). ** $p < 0.01$; ANOVA on linear mixed-effect model, with animal as a random effect. Abbreviations: 3D, three-dimensional; 6-mo, 6-month-old; 14-mo, 14-month-old; ANOVA, analysis of variance; dML, dorsal Molecular Layer; SEM, standard error of the mean. (For interpretation of the references to color in this figure legend, the reader is referred to the Web version of this article.)

Fig. 2C) and in the maximum reached extension (14-mo: 49.56 ± 9.02 µm, 6-mo: 42.18 ± 7.63 µm, $p = 0.003$; Fig. 2C).

3.3. In dorsal hilus astrocyte complexity is not influenced by aging

In the dorsal hilus, unlike what we observed in dGCL and dML, arbor complexity of hilar astrocytes was not different in the 2 age groups (Fig. 3B and C), suggesting no effect of aging in this hippocampal subregion.

3.4. In the dorsal stratum Lacunosum Moleculare, astrocytes exhibit an age-related increase in their morphological complexity

We also looked outside DG, in another dorsal hippocampal subregion which is regarded vulnerable to aging, namely the dorsal sLM (dsLM) of the hippocampus, a synapse-rich region where hippocampal internal interneurons and afferent neuronal inputs from the EC make connections (Deng et al., 2006). Here, astrocytic complexity was also significantly increased in 14-mo versus 6-mo mice as assessed by SIP comparison for the number of intersections at 5–20 µm from the soma (Fig. 4B), as well as for the total number of intersections (14-mo: 30.45 ± 8.97, 6-mo: 20.44 ± 5.53, $p = 0.008$; Fig. 4C). At middle age, compared to younger mice, astrocytes displayed an increase in the total process length (14-mo: 212.89 ± 73.23 µm, 6-mo: 141.82 ± 35.71 µm, $p = 0.003$; Fig. 4C), number of processes (14-mo: 14.20 ± 5.21, 6-mo: 9.85 ± 2.41, $p = 0.004$; Fig. 4C), and in their maximum extension (14-mo: 35.32 ± 6.34 µm, 6-mo: 31.86 ± 7.45 µm, $p = 0.039$; Fig. 4C).

3.5. In entorhinal cortex of middle-aged mice, astrocytes undergo remarkable reduction of their morphological complexity

Finally, in our analysis we included the EC which represents the principal cortical input to the hippocampus and the major input to the dHp (Witter et al., 2013). Here, in contrast with the dGCL, dorsal LM and dsLM, astrocytes in middle-aged animals showed a remarkable reduction in their complexity compared to 6-mo mice (Fig. 5A). Sholl analysis indicated a significant age-related decrease in the numbers of intersections which occurred between 15 and 45 µm from somata (Fig. 5B). Moreover, SIP pointed out a shift in the intersections curve to the left in 14-mo mice. Indeed, in older mice astrocytes, the radius of

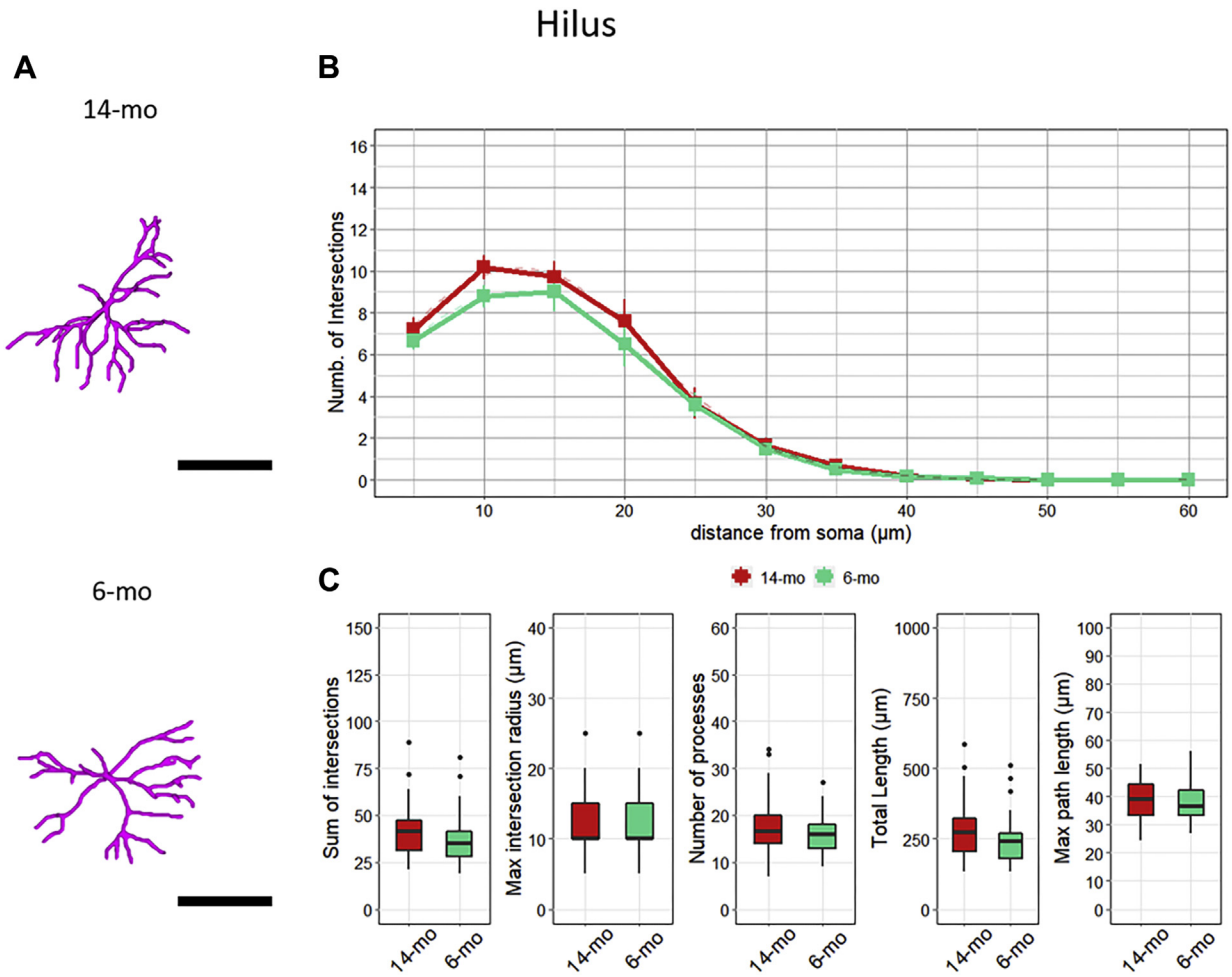

Fig. 3. Aging does not affect the morphology of astrocytes in the hilar region of the dorsal Dentate Gyrus. (A) Representative 3D morphological reconstruction of astrocyte in the Hilus of 14-mo (upper panel) and 6-mo (lower panel) mice, scale bar: 25 µm. (B) Sholl intersection profiles show that astrocytic complexity in Hilus was not affected by age. Color legend: green, 6-mo mice; red, 14-mo mice. Data are presented as mean ± SEM. Nested ANOVA on linear mixed-effect model, with animal as a random effect. (C) Summary of morphometric parameters illustrating the total number of intersections, the distance from the somata with the higher number of intersections, the number of astrocytic processes, total processes length, and the maximum reached extension. In each box plot, the heavy line represents the sample median, the box demarks the range from 25% to 75% of the data, limits of vertical lines (whiskers) represent the minimum and maximum values, excluding outliers (dots). ANOVA on linear mixed-effect model, with animal as a random effect. Abbreviations: 3D, three-dimensional; 6-mo, 6-month-old; 14-mo, 14-month-old; ANOVA, analysis of variance; SEM, standard error of the mean. (For interpretation of the references to color in this figure legend, the reader is referred to the Web version of this article.)

highest count of intersections was significantly decreased, indicating that they reached their maximum complexity closer to somata compared to younger animals (14-mo: 14.33 ± 4.46 µm; 6-mo: 18.75 ± 4.06 µm, $p = 0.002$; Fig. 5C). Marked atrophy of astrocytes in this subarea was also proven by a decrease in the total process length (14-mo: 316.01 ± 155.05 µm, 6-mo: 490.89 ± 148.97 µm, $p = 0.001$; Fig. 5C), in the number of processes (14-mo: 18.21 ± 8.65, 6-mo: 28.21 ± 8.80, $p = 0.0007$; Fig. 5C) together with a reduction in their maximum extension (14-mo: 42.42 ± 8.46 µm, 6-mo: 49.61 ± 7.60 µm, $p = 0.015$; Fig. 5C).

3.6. Regional and subregional differences in the morphological complexity of astrocytes within experimental age groups

To further understand the different age sensitivity of GFAP$^+$ astrocytes in dHp and vHp, we also analyzed differences in astrocyte morphology among subregions, within the 2 age groups. First, we compared astrocytes within the DG subfields in 6-mo male mice (Fig. 6A). Sholl analysis of astrocytes from GCL and ML revealed a similar profile among those subregions of DG (for detailed statistical analysis values see Supplementary table S1 and S2). Hilar astrocytes showed significant differences in SIP profile and a reduced complexity of morphological parameters compared to dGCL (for detailed statistical analysis values see Supplementary table S1 and S2). No difference was observed in comparison with ML astrocytes (for detailed statistical analysis values see Supplementary table S1 and S2). In the hippocampal sLM, astrocytes displayed the least complex structure compared to the other regions. Finally, the EC astrocytes showed the highest number of intersections and reached their maximum complexity at a higher distance from the soma compared to astrocytes from other regions (for detailed statistical analysis values see Supplementary table S1 and S2). In middle-aged mice, astrocytes from GCL and ML showed comparable SIP (Fig. 6B). Moreover, astrocytes from those 2 DG subfields reached the maximum complexity among the 5 subfields under analysis. At 14 months of age astrocytes in the hilus indicated a reduced morphological complexity compared to GCL and ML. Astrocytes in the sLM displayed the least degree of morphological complexity compared to the other fields (for detailed statistical analysis values, see Supplementary table S1 and S2).

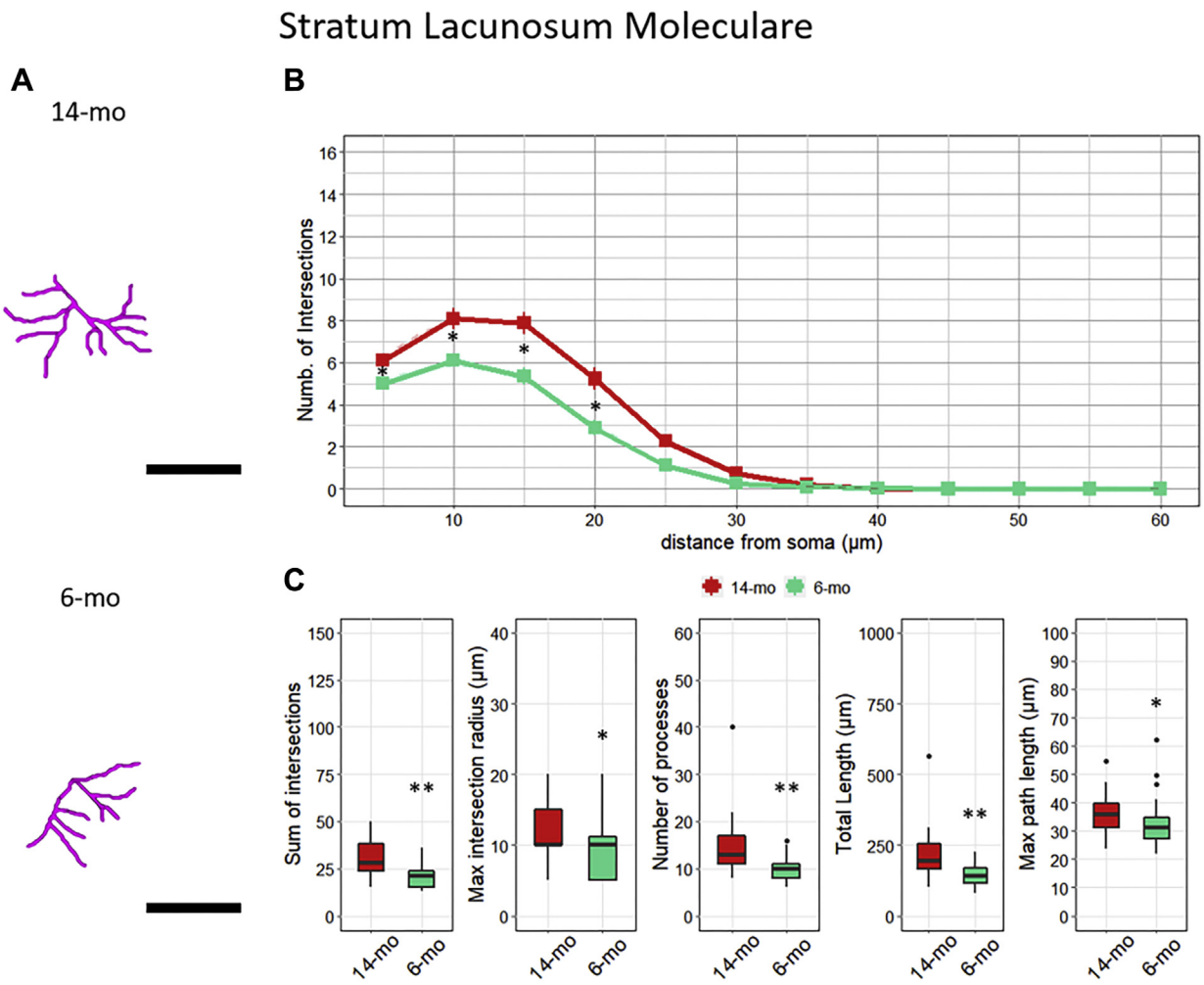

Fig. 4. Astrocytes in the sLM show an age-related increase in their morphological complexity. (A) Representative 3D morphological reconstruction of astrocyte in the sLM region of 14-mo (upper panel) and 6-mo (lower panel) mice, scale bar 25 µm. (B) Sholl intersection profiles show that astrocytic complexity in sLM was significantly increased in 14-mo (red) versus 6-mo (green) mice. Data are presented as mean ± SEM. * $p < 0.05$; nested ANOVA on linear mixed-effect model with animal as a random effect. (C) Summary morphometric parameters illustrating the total number of intersections, the distance from the somata with the higher number of intersections, the number of astrocytic processes, total processes length, and the maximum reached extension. In each box plot, the heavy line represents the sample median, the box demarks the range from 25% to 75% of the data, and limits of vertical lines (whiskers) represent the minimum and maximum values, excluding outliers (dots). * $p < 0.05$, ** $p < 0.01$; ANOVA on linear mixed-effect model with animal as a random effect. Abbreviations: 3D, three-dimensional; 6-mo, 6-month-old; 14-mo, 14-month-old; ANOVA, analysis of variance; SEM, standard error of the mean; sLM, stratum Lacunosum Moleculare. (For interpretation of the references to color in this figure legend, the reader is referred to the Web version of this article.)

Altogether, our data suggested that in the dHp astrocytes undergo complex region-specific morphological changes upon aging, at least in middle-aged mice. Specifically, GFAP$^+$ astrocytes increased their morphological complexity in dGCL, dML, and dsLM, while no change occurred in the hilus.

3.7. In ventral GCL (vGCL) and ML (vML), astrocytes have similar complexity in young and middle-aged mice

Since the dorsal and ventral regions of the DG are considered functionally distinct, with dHp more involved in cognition, we also investigated the potential effects of aging on the ventral pole of DG. Interestingly, astrocytes in the vGCL of the DG, did not display any statistically significant age-related alterations in their morphology (Fig. 7A–C). Also, in the vML, no difference in astrocyte morphology was observed between the 2 ages (Fig. 8A–C), suggesting again no effect of aging in the ventral part of the DG, at least in these 2 subregions.

3.8. Morphological comparison between astrocytes in the dorsal versus ventral dentate gyrus

To further understand the remarkably different age sensitivity of GFAP$^+$ astrocytes in dHp and vHp, we also analyzed astrocyte morphology along the dorsal-ventral axis of the DG within each age group. In 6-mo mice, the morphometric features of astrocytes in dGCL and vGCL were very similar (Fig. 9A), as denoted by no significant difference in the Sholl analysis. Only the maximum reached extension was significant higher in vGCL than dGCL (dGCL: 46.55 ± 8.68 µm, vGCL: 50.65 ± 9.26 µm, $p = 0.028$). Conversely, in 14-mo mice, dGCL astrocytes displayed a more complex morphology than in the vGCL (Fig. 9B). Specifically, in the dGCL astrocytes showed higher number of intersections (dGCL: 62.55 ± 17.16, vGCL: 55.52 ± 19.46, $p = 0.038$), greater arborization (dGCL: 428.27 ± 115.54 µm, vGCL: 375.10 ± 127.84 µm, $p = 0.018$), and longer reached extension (dGCL: 51.05 ± 10.22 µm, vGCL: 47.24 ± 9.00 µm, $p = 0.028$). In the ML, the morphological differences described in dHp versus vHp were even more consistent. In 6-mo mice,

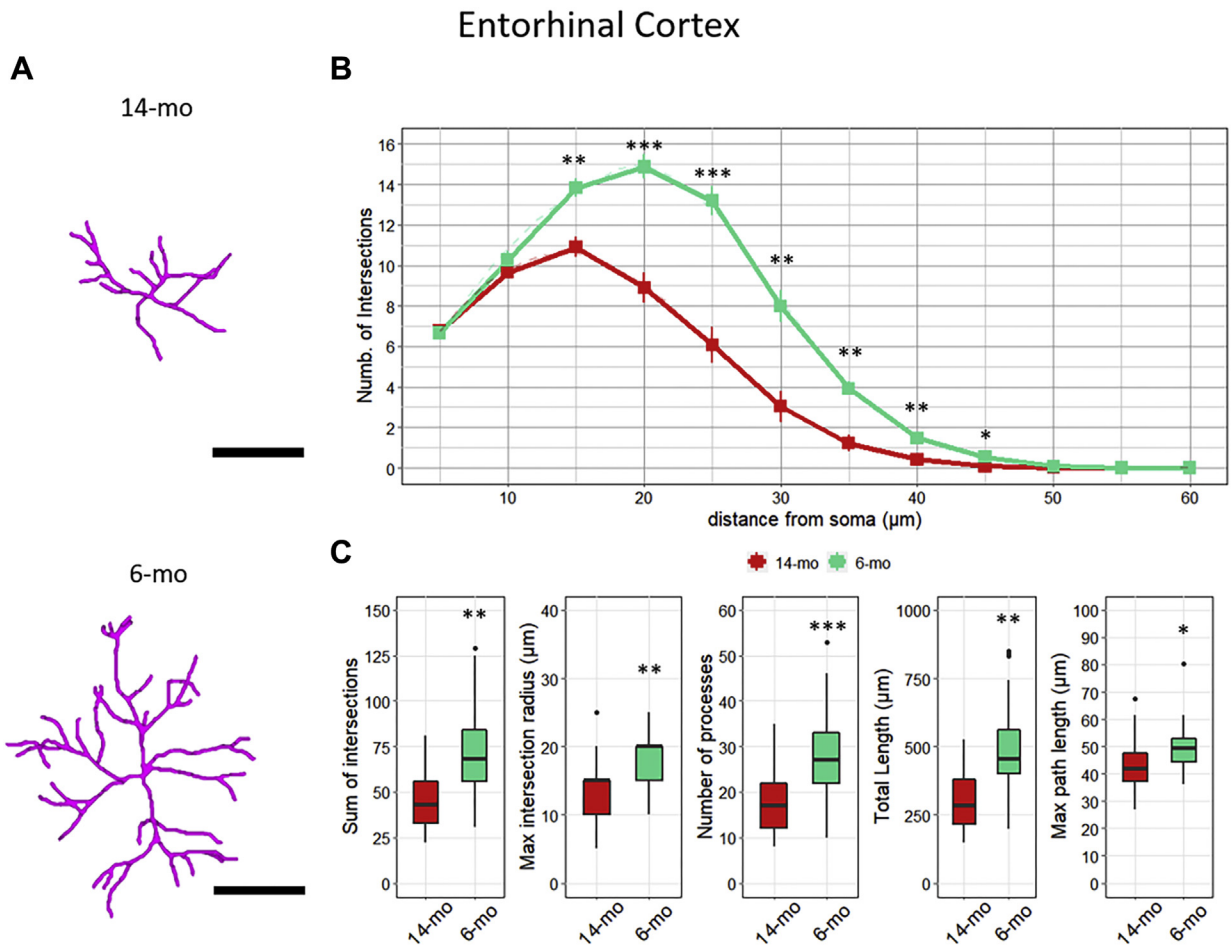

Fig. 5. Middle-aged mice display a reduced morphological complexity of EC astrocytes. (A) Representative 3D morphological reconstruction of astrocyte in the EC of 14-mo (upper panel) and 6-mo (lower panel) mice, scale bar 25 µm. (B) Sholl intersection profiles show that astrocytic complexity in EC was significantly decreased in 14-mo (red) versus 6-mo (green) mice. Data are presented as mean ± SEM. * $p < 0.05$, ** $p < 0.01$, *** $p < 0.001$; nested ANOVA on linear mixed-effect model, with animal as a random effect. (C) Summary of morphometric parameters illustrating the total number of intersections, the distance from the somata with the higher number of intersections, the number of astrocytic processes, total processes length, and the maximum reached extension. In each box plot, the heavy line represents the sample median, the box demarks the range from 25% to 75% of the data, and limits of vertical lines (whiskers) represent the minimum and maximum values, excluding outliers (dots). * $p < 0.05$, ** $p < 0.01$, *** $p < 0.001$; ANOVA on linear mixed-effect model, with animal as a random effect. Abbreviations: 3D, three-dimensional; 6-mo, 6-month-old; 14-mo, 14-month-old; ANOVA, analysis of variance; EC, entorhinal cortex; SEM, standard error of the mean. (For interpretation of the references to color in this figure legend, the reader is referred to the Web version of this article.)

astrocytes in the vML were more complex than those in the dML (Fig. 10A), as indicated by SIP curves and Sholl-related morphological features. Higher complexity of astrocytes in vML was also underlined by greater arborization (dML: 255.21 ± 68.48 µm, vML: 286.81 ± 65.18 µm, $p = 0.014$) and higher number of processes (dML: 15.08 ± 4.42, vML: 18.54 ± 4.71, $p < 0.001$). With aging, we described a reverse situation, where the dML is the region where astrocytes displayed more complex morphology (Fig. 10B). The analysis of SIP indicated higher complexity between 10 and 40 µm from soma in dML compare to vML. Moreover, the total number of intersections (dML: 57.68 ± 13.98, vML: 45.92 ± 12.59, $p < 0.001$), the total length (dML: 382.78 ± 87.38 µm, vML: 304.91 ± 75.92 µm, $p < 0.001$), the number of processes (dML: 21.60 ± 5.47, vML: 19.17 ± 5.29, $p = 0.014$), and maximum reached extension (dML: 49.56 ± 9.02 µm, vML: 45.05 ± 7.48 µm, $p = 0.003$) were higher in the dML compared to vML.

4. Discussion

Previous reports demonstrated that extensive morphological and functional remodeling of astrocytes occurs during aging. Among other changes, aging has been associated with reduced astroglial coverage of synapses and synthesis of synaptogenic factors, decreased astroglial metabolic support to neurons, reduced astroglial-vascular coupling, and reduced ability to mount reactive astrogliosis (as recently reviewed by Verkhratsky et al., 2020). Altogether these changes potentially contribute to the idea that astroglial loss of homeostatic function or asthenia, rather than increased reactivity, may prevail during brain aging.

It is generally agreed that physiological aging is not associated with changes in the number of astrocytes across distinct CNS regions, including the hippocampus (Long et al., 1998). On the other hand, as far as morphological astrocytic changes during aging, both increased and decreased size and complexity have been reported, with the majority of studies using GFAP for immunolabeling (Verkhratsky et al., 2020).

In recent years, next-generation sequencing techniques allowed a broad characterization of the transcriptional changes occurring specifically in astrocytes during aging. Such efforts contribute to the idea of different susceptibility of specific brain regions to aging-induced alteration of astrocytic gene expression and functions (Boisvert et al., 2018; Clarke et al., 2018). Although a topic still in its infancy, current and future knowledge on regional specificity of age-associated glial changes may help understanding why discrete

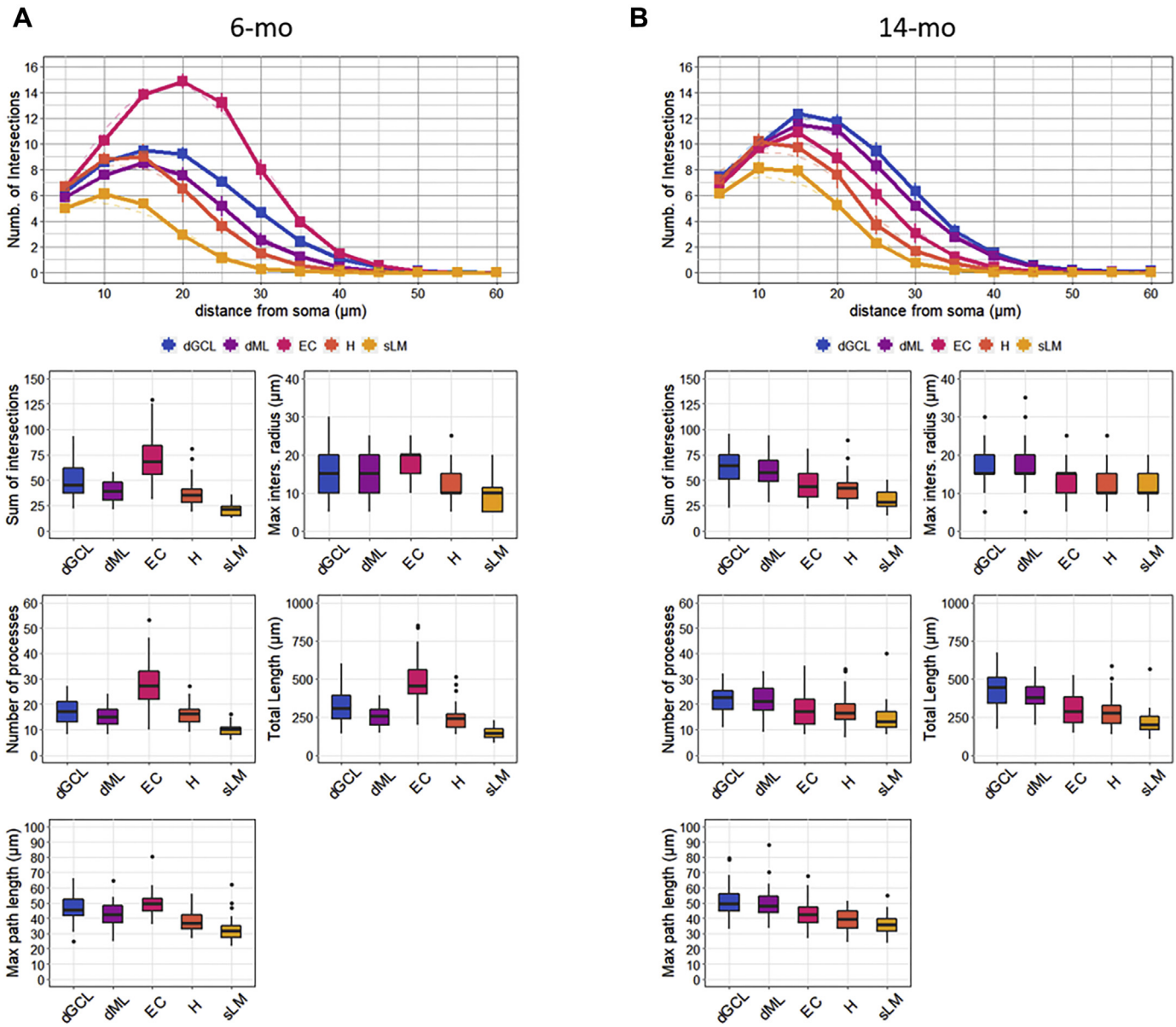

Fig. 6. Regional and sub-regional differences in the morphological complexity of astrocytes within experimental age groups. SIPs and morphological features of astrocytes from 6-mo (A) and 14-mo (B) mice. For SIP, data are presented as mean ± SEM; nested ANOVA followed by Tukey's HSD test on linear mixed-effect model with animal as a random effect (multiplicity-adjusted *p* values are listed in Supplementary Table S1). In the box plots of morphological parameters, the heavy line represents the sample median, the box demarks the range from 25% to 75% of the data, and limits of vertical lines (whiskers) represent the minimum and maximum values, excluding outliers. ANOVA followed by Tukey's HSD test on linear mixed-effect model with animal as a random effect (multiplicity-adjusted *p* values are listed in Supplementary Table S2). Abbreviations: 6-mo, 6-month-old; 14-mo, 14-month-old; ANOVA, analysis of variance; dGCL, dorsal Granule Cell Layer; dML, dorsal Molecular Layer; EC, entorhinal cortex; H, hilus; SEM, standard error of the mean; SIP, Sholl intersection profile; sLM, stratum Lacunosum Moleculare.

bran regions are more vulnerable to synaptic and neuronal disfunction, to aging and to age-related neurodegenerative disorders (Burke and Barnes, 2010; Verkhratsky et al., 2014).

To investigate the effects of aging on astrocytes within different hippocampal subfields, herein we performed a semi-automated morphological analysis of astrocytes from 6-mo and 14-mo C57BL/6J male mice. More in detail, we performed a computer-based 3D reconstruction of GFAP-immunolabeled astrocytes, and extensively quantified their morphological complexity by Sholl analysis. Moreover, we evaluated additional morphometric features such as number of processes, total length, and maximum process extension (Scorcioni et al., 2008). Although GFAP immunolabeling does not delineate the overall structure of astrocytes and this protein is not expressed by all astrocytes, it still represents a reliable strategy to identify the major morphological features of astrocytes and it has been used and validated in other relevant works (Rodríguez et al., 2014; SheikhBahaei et al., 2016; Tavares et al., 2017; Verkhratsky et al., 2020).

In our study, we initially focused our attention on 3 DG subfields: GCL, ML, and H. Within the DG, astrocytes actively modulate the differentiation, growth, survival, and integration of adult born neuroblasts and neurons (Cassé et al., 2018; Cvijetic et al., 2017; Spampinato et al., 2019). Aging is associated with a progressive decline in the self-renewal and regenerative capacities of CNS stem cells, an occurrence at least in part due to reduced asymmetric division of neural stem/progenitor cells (Nicaise et al., 2020).

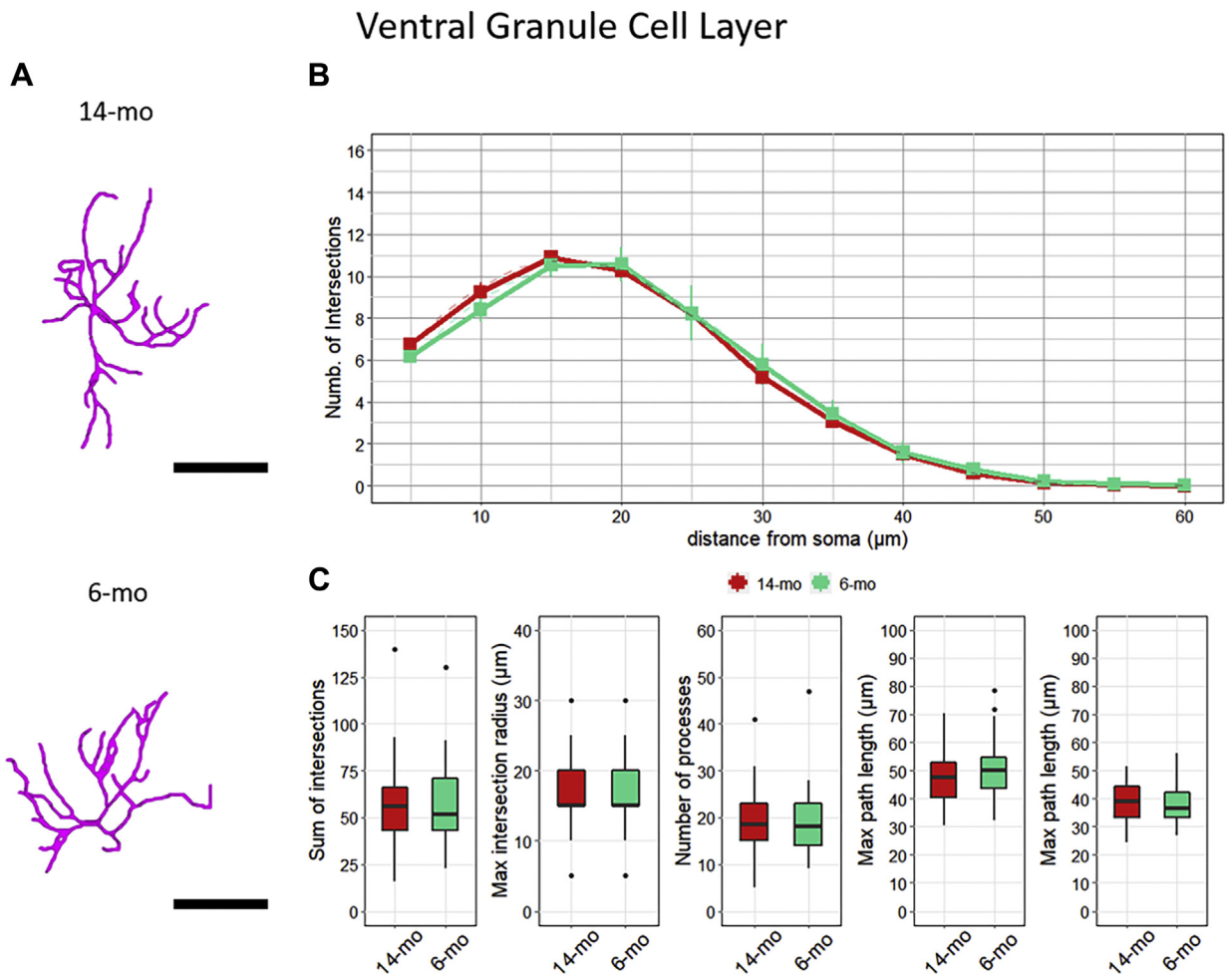

Fig. 7. Aging does not affect the morphological complexity of astrocytes in the vGCL. (A) Representative 3D morphological reconstruction of astrocyte in the vGCL of 14-mo (upper panel) and 6-mo (lower panel) mice, scale bar: 25 µm. (B) Sholl intersection profiles show that astrocytic complexity in vGCL was not affected by age. Color legend: green, 6-mo mice; red, 14-mo mice. Data are presented as mean ± SEM. Nested ANOVA on linear mixed-effect model with animal as a random effect. (C) Summary of morphometric parameters illustrating the total number of intersections, the distance from the somata with the higher number of intersections, the number of astrocytic processes, total processes length, and the maximum reached extension. In each box plot, the heavy line represents the sample median, the box demarks the range from 25% to 75% of the data, and limits of vertical lines (whiskers) represent the minimum and maximum values, excluding outliers (dots). ANOVA on linear mixed-effect model with animal as a random effect. Abbreviations: 3D, three-dimensional; 6-mo, 6-month-old; 14-mo, 14-month-old; ANOVA, analysis of variance; SEM, standard error of the mean; vGCL, ventral region of the Granule Cell Layer. (For interpretation of the references to color in this figure legend, the reader is referred to the Web version of this article.)

Deficient astroglial support to neural stem/progenitor cells and their adult-born progeny may contribute to that decline in the hippocampus (Miranda et al., 2012; Okamoto et al., 2011), again supporting a loss of function for this glial cell type in aging. In dGCL and dML, 14-mo astrocytes showed significantly more complex arborizations than corresponding cells from 6-mo mice. Subregional morphological changes of hippocampal GFAP$^+$ astrocytes during aging were previously investigated by Rodríguez et al. (2014). These authors reported a progressive age-dependent hypertrophy of GFAP$^+$ astrocytes in DG, as indicated by increased surface, volume, and somata size (Rodríguez et al., 2014). Now our morphological analysis provides more detailed information on the increasing morphological complexity of astrocytes during aging specifically in GCL and ML. Our analysis was also extended to the hilus. Here, astrocyte complexity remained remarkably stable in middle-aged compared to young adult mice, with no difference reported in the 2 experimental groups. We also looked outside the DG, in the CA1 region, in the sLM, where astrocytes interact with hippocampal interneurons and afferent fibers from the EC (Witter, 2013). Again, we demonstrated that also sLM astrocytes from 14-mo mice showed a more complex structure than 6-mo mice. Previously published work showed age-dependent hypertrophy in astrocytes within the CA1 region, but no information on the evaluated subfield is available (Rodríguez et al., 2014).

The hippocampus is not a homogenous structure, since anatomical, molecular, and functional segregation occurs along its dorsoventral axis (Fanselow and Dong, 2010; Grilli et al., 1988). Remarkably, no previous studies evaluated astrocytes along the dorsoventral axis by morphometric analysis and in response to aging. For this reason, we performed our analysis in the ventral DG. Surprisingly, in this region we observed no significant difference between 6- and 14-mo mice in both vGCL and vML. Although at present our findings are only descriptive in nature, we believe that it is quite interesting that during aging astrocytic morphological features change only in the dDG.

The dHp has been primarily correlated with cognitive functions, while the vHp is involved in emotional and anxiety-related behaviors (Fanselow and Dong, 2010; Strange et al., 2014). In a unique longitudinal magnetic resonance imaging and behavioral mouse study, Reichel et al. (2017) demonstrated that age-related cognitive decline coincides with accelerated volume loss of the dHp but not vHp. Lee et al. (2017) were first to apply RNA-seq analysis to

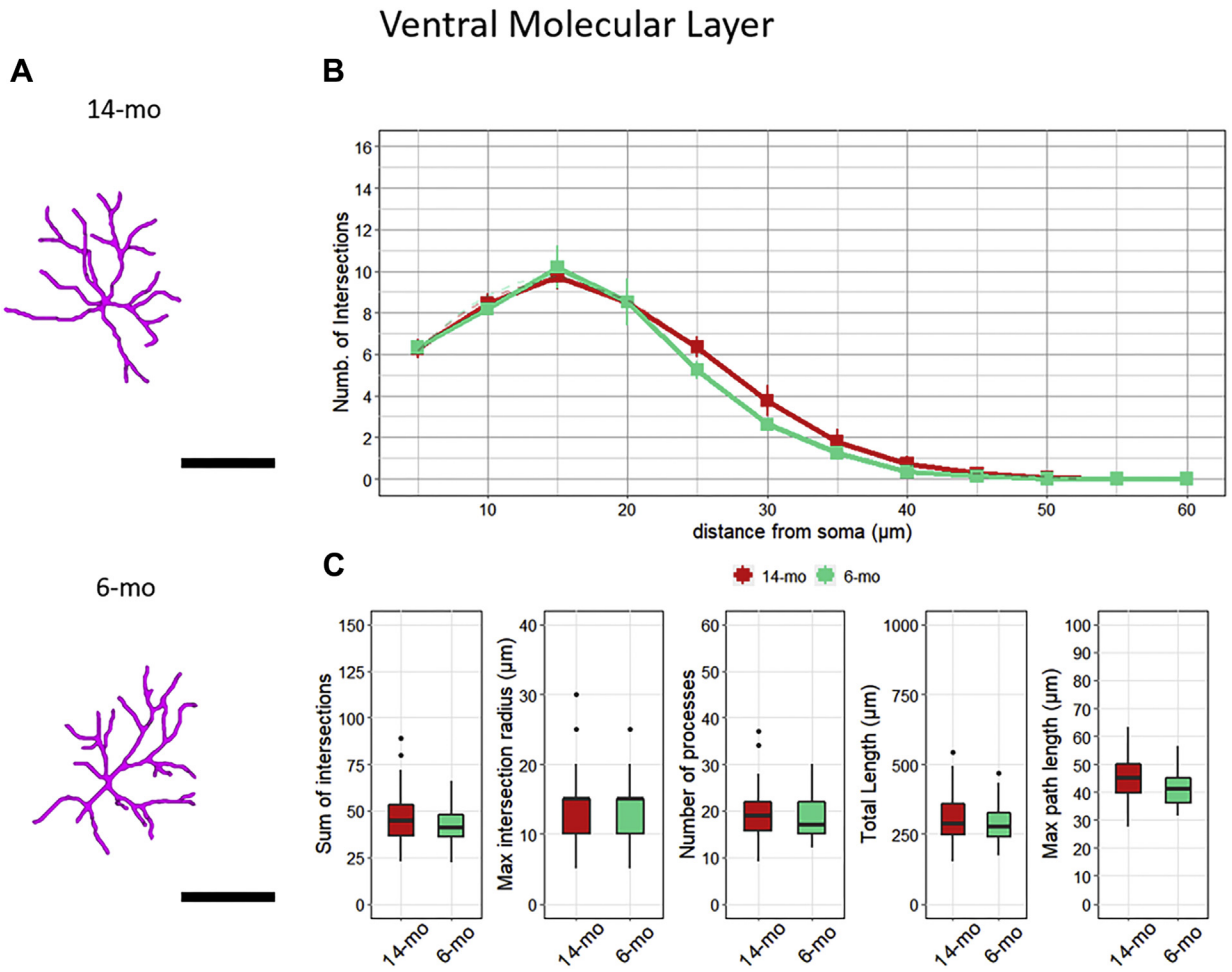

Fig. 8. In the vML, the morphology of astrocytes is not altered by aging. (A) Representative 3D morphological reconstruction of astrocyte in the vML of 14-mo (upper panel) and 6-mo (lower panel) mice, scale bar: 25 µm. (B) Sholl intersection profiles show that astrocytic complexity in vML was not affected by age. Color legend: green, 6-mo mice; red, 14-mo mice. Data are presented as mean ± SEM. Nested ANOVA on linear mixed-effect model with animal as a random effect. (C) Summary of morphometric parameters illustrating the total number of intersections, the distance from the somata with the higher number of intersections, the number of astrocytic processes, total processes length, and the maximum reached extension. In each box plot, the heavy line represents the sample median, the box demarks the range from 25% to 75% of the data, and limits of vertical lines (whiskers) represent the minimum and maximum values, excluding outliers (dots). ANOVA on linear mixed-effect model with animal as a random effect. Abbreviations: 3D, three-dimensional; 6-mo, 6-month-old; 14-mo, 14-month-old; ANOVA, analysis of variance; SEM, standard error of the mean; vML, ventral Molecular Layer. (For interpretation of the references to color in this figure legend, the reader is referred to the Web version of this article.)

investigate transcriptional differences along the hippocampal dorsoventral axis. They demonstrated differentially expressed genes in the dHp and vHp of P14, P28, and P45 mice. Bioinformatic analysis revealed that pathways involving long-term potentiation and the glutamatergic synapses are strongly associated with genes enriched in the dHp, whereas pathways involving the GABAergic synapse and serotonergic synapse are correlated with vHp enriched genes.

Astrocytes instruct the formation, maturation, and elimination of synapses under physiological conditions, and impairment of these functions has been implicated in aging and many aging-related diseases (Verkhratsky et al., 2019, 2020). The age-related changes we have observed in dorsal DG of middle-aged mice are likely not limited to astrocyte morphological appearance but they may be associated with modifications of their activities and functions (Jinno, 2011; Mosher and Schaffer, 2018). Clarke et al. (2018) performed RNA sequencing of astrocytes from different brain regions to identify potential age-related transcriptional changes that could contribute to cognitive decline. They suggested that aged astrocytes may take on a reactive phenotype characteristic of neuroinflammatory astrocytes. In the future, astrocyte RNA sequencing profiles along the dorsoventral hippocampal axis should be investigated for understanding the potential relevance of dorsal-specific changes in cognitive decline.

Astrocytes are also important contributors in the DG neurogenic niche (Cvijetic et al., 2017; Song et al., 2002; Spampinato et al., 2019). Moreover, it has been proposed that age-related decline in the generation of adult-born neurons may contribute to age-dependent deficits in cognitive functions (Bettio et al., 2017; Lazarov et al., 2010). Experimental manipulation of ahNG by environmental stimuli, pharmacological and genetic approaches is associated with changes in cognitive performance in the dDG and with affective behavioral regulation in the vDG (Bortolotto et al., 2019; Bortolotto and Grilli, 2020; Tanti and Belzung, 2013; Vivar et al., 2013). At least in rodents, key differences in neurogenic characteristics have been described along the dorsal-ventral DG axis: for example, dDG exhibits higher levels of neurogenesis and faster rates of newborn neuron maturation than vDG (Jinno, 2016; Piatti et al., 2011; Snyder et al., 2009). Although at this stage we can only speculate, preferential aging-associated astrocytic changes in the dDG, at least in GCL and ML, may, in turn, affect the dorsal neurogenic microenvironment and potentially contribute to age-related defective NG and cognitive decline. For example, with aging, astrocytes produce lower levels of key secreted proteins,

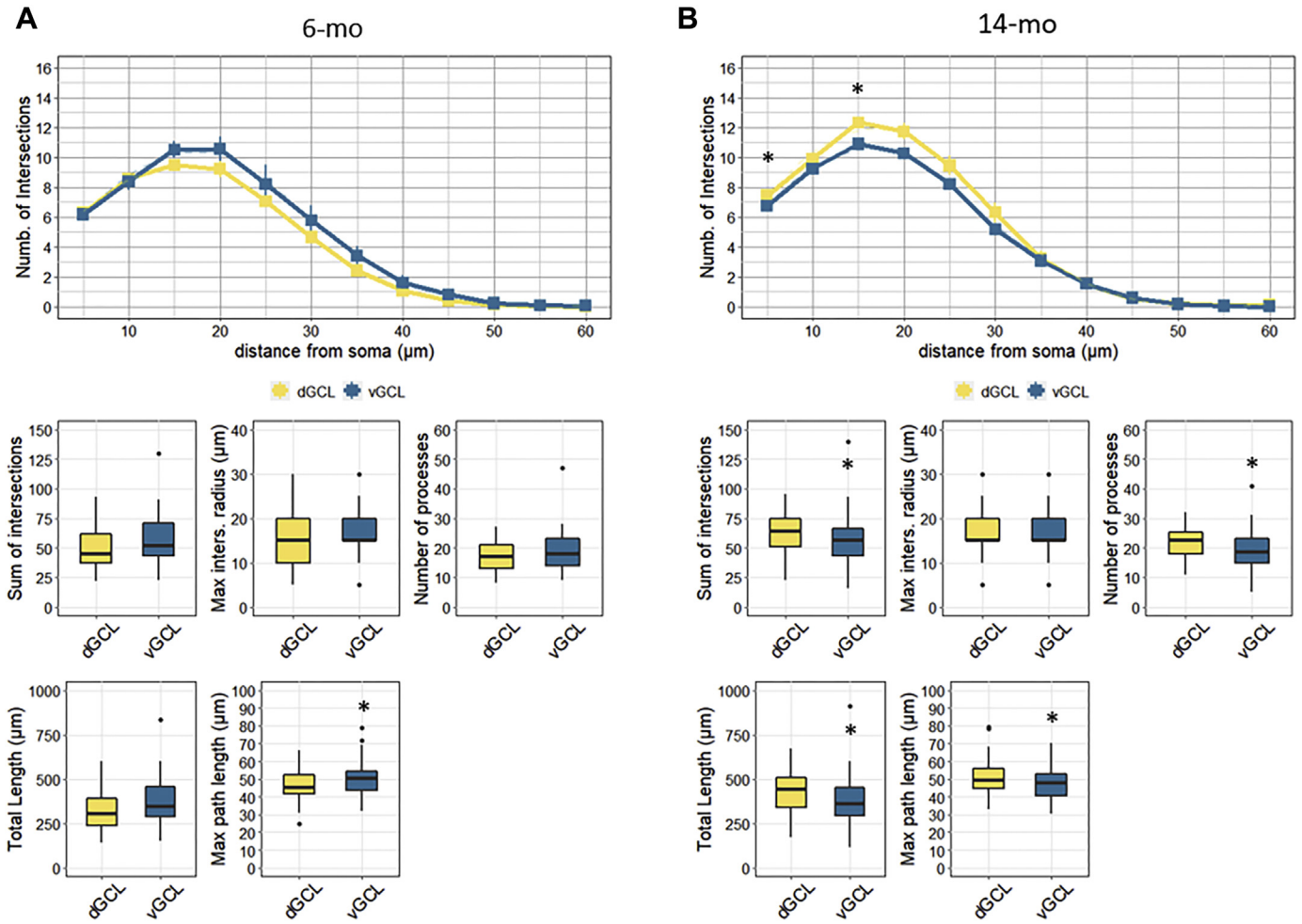

Fig. 9. Morphological differences between astrocytes in the dorsal versus ventral Granule Cell Layer within each age group. SIPs and morphological features of astrocytes from 6-mo (A) and 14-mo (B) mice. For SIP, data are presented as mean ± SEM. * $p < 0.05$; nested ANOVA on linear mixed-effect model, with animal as a random effect. In the box plots of morphological parameters, the heavy line represents the sample median, the box demarks the range from 25% to 75% of the data, and limits of vertical lines (whiskers) represent the minimum and maximum values, excluding outliers. * $p < 0.05$; ANOVA on linear mixed-effect model, with animal as a random effect. Color code: blue, vGCL; yellow, dGCL. Abbreviations: 3D, three-dimensional; 6-mo, 6-month-old; 14-mo, 14-month-old; ANOVA, analysis of variance; dGCL, dorsal Granule Cell Layer; SEM, standard error of the mean; SIP, Sholl intersection profile; vGCL, ventral region of the Granule Cell Layer. (For interpretation of the references to color in this figure legend, the reader is referred to the Web version of this article.)

including several growth factors (Mosher and Schaffer, 2018). Potentially, this may influence proliferation and differentiation of adult neural stem/progenitor cells and it may be involved in age-related decline in adult neurogenesis (Mosher and Schaffer, 2018). Alterations in cell to cell contact within the dHp neurogenic niche can also be envisioned as a result of the morphological changes we have described in middle-aged mice and, potentially, negatively affect ahNG. Again, the use of next-generation sequencing, in combination with proteomic approaches, may help unravel the biological basis of aging associated changes.

To further explore the potential differences between astrocytes along the dorsoventral pole of DG, in our study we have compared astrocyte morphology of dorsal and ventral GCL and ML subregions within each age group. In 6-mo animals, astrocyte complexity in the vGCL and dGCL was very similar. On the contrary, in the ML we observed remarkable difference along the dorsoventral axis of DG. More specifically, astrocytes in the vML are more complex, with higher arborization length and branching than astrocytes in the dML. With aging, we described a reverse situation, where the dML was the subregion where astrocytes displayed highest complexity. We were also able to compare astrocytes among different DG subregions. In 6-mo mice, morphological analysis of astrocytes in the 3 dDG subfields (dGCL, dML, and H) indicated that these cells show a similar grade of complexity. In the sLM, astrocytes displayed the lowest morphological complexity compared to the other subfields. Similar morphological complexity was observed at 6 and 14 months of age between astrocytes in dGCL and dML. In dDG subfields, astrocytes reached the highest complexity at 14 months. At this age, hilar astrocytes showed reduced morphological complexity compared to astrocytes in the other dDG subfields. To the best of our knowledge, this is the first study where such astrocytic morphological differences within different hippocampal subfields are described. Very recently, Popov et al. (2020) evaluated the morphology of astrocytes in hippocampal slices of young, adult, and old mice by 2 photon imaging and volume fraction analysis. The authors demonstrated a decrease in astrocytic domain size, volume fraction of perisynaptic processes, and astrocyte coupling through gap-junctions in aging. Interestingly, these astrocytic changes correlated with disrupted K^+ buffering, glutamate clearance, and astrocytic Ca^{2+} signaling which, in turn, impacted on synaptic plasticity and long-term potentiation in hippocampal synapses (Popov et al., 2020). At this stage of knowledge, our results of distinct morphological changes in DG subfields are descriptive in nature. In the future, we should try to correlate age-dependent

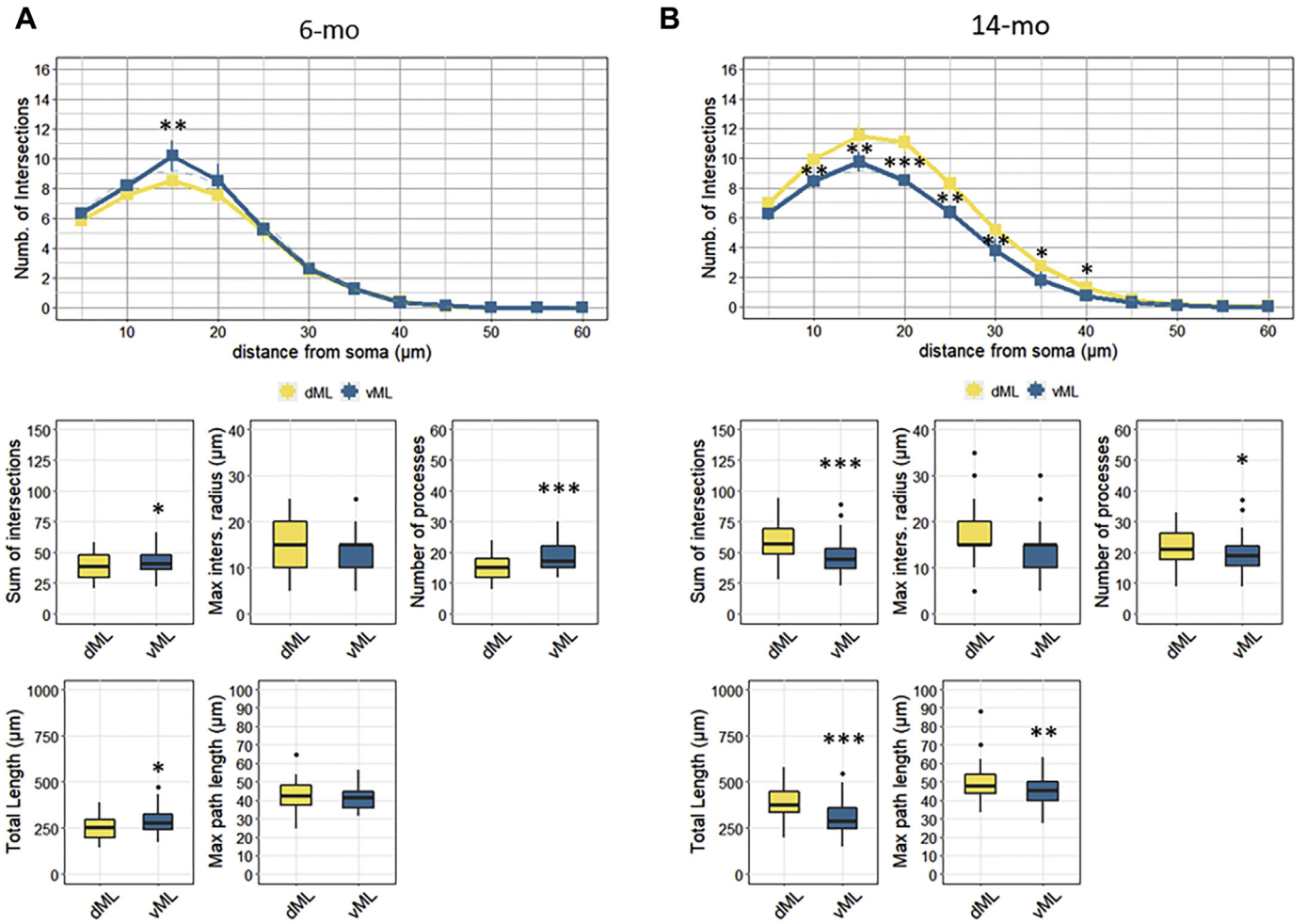

Fig. 10. Morphometric differences between astrocytes in the dorsal versus ventral Molecular Layer within each age group. SIPs and morphological features of astrocytes from 6-mo (A) and 14-mo (B) mice. For SIP, data are presented as mean ± SEM. * $p < 0.05$, ** $p < 0.01$, *** $p < 0.001$; nested ANOVA on linear mixed-effect model, with animal as a random effect. In the box plots of morphological parameters, the heavy line represents the sample median, the box demarks the range from 25% to 75% of the data, and limits of vertical lines (whiskers) represent the minimum and maximum values, excluding outliers. * $p < 0.05$, ** $p < 0.01$, *** $p < 0.001$; ANOVA on linear mixed-effect model, with animal as a random effect. Color code: blue, vML; yellow, dML. Abbreviations: 3D, three-dimensional; 6-mo, 6-month-old; 14-mo, 14-month-old; ANOVA, analysis of variance; dML, dorsal Molecular Layer; SEM, standard error of the mean; SIP, Sholl intersection profile; vML, ventral Molecular Layer. (For interpretation of the references to color in this figure legend, the reader is referred to the Web version of this article.)

morphological changes with astrocytic physiology in dorsal versus ventral DG and in different hippocampal subfields.

Interestingly, EC, which is the major input to the dorsal DG, was also a region where morphological changes occurred and the only region where we documented remarkable atrophy in 14-mo mice. Of note, at 6 months of age, EC astrocytes resulted structurally much more complex than astrocytes residing in any other tested region. Specifically, they have the highest process length and number and their processes reach their maximum complexity more distant from the soma. EC plays an essential role in cognition and memory and it is among the earliest brain regions affected by AD-related pathology (Braak et al., 1993). The remarkable alterations of EC astroglial cells in middle-aged mice are in agreement with previous reports of their reduced surface and volume (Rodríguez et al., 2014), and may also be relevant to age-related cognitive decline. Again, a more systematic research is needed to elucidate if and how opposite morphological changes (increased or decreased structural complexity) may be linked to region-specific synapse and neuronal dysfunction/loss and cognitive deficits.

In conclusion, herein we describe, for the first time, remarkable heterogeneity in the astrocytic response to aging mainly in the dorsal, and not ventral, DG and in different subfields within dorsal DG and CA1. Since dorsal, and not ventral, hippocampus is involved in cognitive functions, these findings appear worth of further evaluation. Our findings also provide an additional level of complexity in the structural changes associated with physiological brain aging. Aging is also considered a key risk factor for devastating neurodegenerative disorders, such as Alzheimer's disease and Parkinson's disease. It may be interesting to evaluate whether a dorsal specificity in astrocytic changes may also occur in neurodegenerative animal models, their correlation with cognitive performance, and, potentially, their response to drugs. Last but not least, it should also be underlined that our studies were performed in male mice. In the future detailed evaluation of age-dependent changes in astrocyte morphological complexity in different brain regions/subfields should be undertaken in female mice to verify if sex-related differences may also exist.

Disclosure statement

The authors declare no conflict of interest.

CRediT authorship contribution statement

Heather Bondi: Methodology, Investigation, Formal analysis, Visualization, Writing - original draft. **Valeria Bortolotto:** Resources, Writing - original draft. **Pier Luigi Canonico:** Data curation, Funding acquisition. **Mariagrazia Grilli:** Conceptualization, Methodology, Writing - original draft, Supervision, Funding acquisition.

Acknowledgements

This work was partially supported by PRIN 2017 (grant number 2017MYJ5TH_003). HB held a research fellowship (Bando Fondazione CRT, ID 393) supported by the University of Piemonte Orientale, Italy.

Appendix A. Supplementary data

Supplementary data to this article can be found online at https://doi.org/10.1016/j.neurobiolaging.2020.12.018.

References

Augusto-Oliveira, M., Arrifano, G.P., Takeda, P.Y., Lopes-Araújo, A., Santos-Sacramento, L., Anthony, D.C., Verkhratsky, A., Crespo-Lopez, M.E., 2020. Astroglia-specific contributions to the regulation of synapses, cognition and behaviour. Neurosci. Biobehav. Rev. 118, 331–357.
Bates, D., Mächler, M., Bolker, B., Walker, S., 2015. Fitting linear mixed-effects models using lme4. J. Stat. Softw. 67, 1–48.
Bettio, L.E.B., Rajendran, L., Gil-Mohapel, J., 2017. The effects of aging in the hippocampus and cognitive decline. Neurosci. Biobehav. Rev. 79, 66–86.
Boisvert, M.M., Erikson, G.A., Shokhirev, M.N., Allen, N.J., 2018. The aging astrocyte transcriptome from multiple regions of the mouse brain. Cell Rep. 22, 269–285.
Bortolotto, V., Bondi, H., Cuccurazzu, B., Rinaldi, M., Canonico, P.L., Grilli, M., 2019. Salmeterol, a β2 adrenergic agonist, promotes adult hippocampal neurogenesis in a region-specific manner. Front Pharmacol. 10, 1000.
Bortolotto, V., Grilli, M., 2020. Activation of β2 adrenergic receptors promotes adult hippocampal neurogenesis. Neural Regen. Res. 15, 2258.
Braak, H., Braak, E., Bohl, J., 1993. Staging of Alzheimer-related cortical destruction. Eur. Neurol. 33, 403–408.
Burger, C., 2010. Region-specific genetic alterations in the aging hippocampus: implications for cognitive aging. Front Aging Neurosci. 2, 140.
Burke, S.N., Barnes, C.A., 2010. Senescent synapses and hippocampal circuit dynamics. Trends Neurosci. 33, 153–161.
Cassé, F., Richetin, K., Toni, N., 2018. Astrocytes' contribution to adult neurogenesis in physiology and Alzheimer's disease. Front Cell Neurosci 12, 432.
Clarke, L.E., Liddelow, S.A., Chakraborty, C., Münch, A.E., Heiman, M., Barres, B.A., 2018. Normal aging induces A1-like astrocyte reactivity. Proc. Natl. Acad. Sci. U. S. A. 115, E1896–E1905.
Cvijetic, S., Bortolotto, V., Manfredi, M., Ranzato, E., Marengo, E., Salem, R., Canonico, P.L., Grilli, M., 2017. Cell autonomous and noncell-autonomous role of NF-κB p50 in astrocyte-mediated fate specification of adult neural progenitor cells. Glia 65, 169–181.
Dahan, L., Rampon, C., Florian, C., 2020. Age-related memory decline, dysfunction of the hippocampus and therapeutic opportunities. Prog. Neuropsychopharmacol. Biol. Psychiatry 102, 109943.
Deng, J.B., Yu, D.M., Li, M.S., 2006. Formation of the entorhino-hippocampal pathway: a tracing study in vitro and in vivo. Neurosci. Bull 22, 305–314.
Fanselow, M.S., Dong, H.W., 2010. Are the dorsal and ventral hippocampus functionally distinct structures? Neuron 65, 7–19.
Ferreira, T.A., Blackman, A.V., Oyrer, J., Jayabal, S., Chung, A.J., Watt, A.J., Sjöström, P.J., van Meyel, D.J., 2014. Neuronal morphometry directly from bitmap images. Nat. Methods 11, 982–984.
Geinisman, Y., Detoledo-Morrell, L., Morrell, F., Heller, R.E., 1995. Hippocampal markers of age-related memory dysfunction: behavioral, electrophysiological and morphological perspectives. Prog. Neurobiol. 45, 223–252.
Grilli, M., Nisoli, E., Memo, M., Missale, C., Spano, P.F., 1988. Pharmacological characterization of D1 and D2 dopamine receptors in rat limbocortical areas. II. Dorsal hippocampus. Neurosci. Lett. 87, 253–258.
Hothorn, T., Bretz, F., Westfall, P., 2008. Simultaneous inference in general parametric models. Biom. J. 346–363.
Jinno, S., 2011. Regional and laminar differences in antigen profiles and spatial distributions of astrocytes in the mouse hippocampus, with reference to aging. Neuroscience 180, 41–52.
Jinno, S., 2016. Aging affects new cell production in the adult hippocampus: a quantitative anatomic review. J. Chem. Neuroanat. 76, 64–72.
Lazarov, O., Mattson, M.P., Peterson, D.A., Pimplikar, S.W., van Praag, H., 2010. When neurogenesis encounters aging and disease. Trends Neurosci. 33, 569–579.
Lee, A.R., Kim, J.H., Cho, E., Kim, M., Park, M., 2017. Dorsal and ventral hippocampus differentiate in functional pathways and differentially associate with neurological disease-related genes during postnatal development. Front Mol. Neurosci. 10, 331.
Long, J.M., Kalehua, A.N., Muth, N.J., Calhoun, M.E., Jucker, M., Hengemihle, J.M., Ingram, D.K., Mouton, P.R., 1998. Stereological analysis of astrocyte and microglia in aging mouse hippocampus. Neurobiol. Aging 19, 497–503.
Longair, M.H., Baker, D.A., Armstrong, J.D., 2011. Simple neurite tracer: open source software for reconstruction, visualization and analysis of neuronal processes. Bioinformatics 27, 2453–2454.
Matias, I., Morgado, J., Gomes, F.C.A., 2019. Astrocyte heterogeneity: impact to brain aging and disease. Front Aging Neurosci. 11, 59.
Miranda, C.J., Braun, L., Jiang, Y., Hester, M.E., Zhang, L., Riolo, M., Wang, H., Rao, M., Altura, R.A., Kaspar, B.K., 2012. Aging brain microenvironment decreases hippocampal neurogenesis through Wnt-mediated survivin signaling. Aging Cell 11, 542–552.
Mosher, K.I., Schaffer, D.V., 2018. Influence of hippocampal niche signals on neural stem cell functions during aging. Cell Tissue Res 371, 115–124.
Mota, C., Taipa, R., das Neves, S.P., Monteiro-Martins, S., Monteiro, S., Palha, J.A., Sousa, N., Sousa, J.C., Cerqueira, J.J., 2019. Structural and molecular correlates of cognitive aging in the rat. Sci. Rep. 9.
Nicaise, A.M., Willis, C.M., Crocker, S.J., Pluchino, S., 2020. Stem cells of the aging brain. Front Aging Neurosci.
Okamoto, M., Inoue, K., Iwamura, H., Terashima, K., Soya, H., Asashima, M., Kuwabara, T., 2011. Reduction in paracrine Wnt3 factors during aging causes impaired adult neurogenesis. FASEB J. 25, 3570–3582.
Palmer, A.L., Ousman, S.S., 2018. Astrocytes and aging. Front Aging Neurosci. 10, 337.
Paxinos, G., Franklin, K.B.J., 2004. In: The Mouse Brain in Stereotaxic Coordinates, second ed. Elsevier Academic, London.
Piatti, V.C., Davies-Sala, M.G., Espósito, M.S., Mongiat, L.A., Trinchero, M.F., Schinder, A.F., 2011. The timing for neuronal maturation in the adult hippocampus is modulated by local network activity. J. Neurosci. 31, 7715–7728.
Popov, A., Brazhe, A., Denisov, P., Sutyagina, O., Lazareva, N., Verkhratsky, A., Semyanov, A., 2020. Astrocytes dystrophy in ageing brain parallels impaired synaptic plasticity. bioRxiv.
Reichel, J.M., Bedenk, B.T., Czisch, M., Wotjak, C.T., 2017. Age-related cognitive decline coincides with accelerated volume loss of the dorsal but not ventral hippocampus in mice. Hippocampus 27, 28–35.
Rodríguez, J.J., Yeh, C.Y., Terzieva, S., Olabarria, M., Kulijewicz-Nawrot, M., Verkhratsky, A., 2014. Complex and region-specific changes in astroglial markers in the aging brain. Neurobiol. Aging 35, 15–23.
Rosenzweig, E.S., Barnes, C.A., 2003. Impact of aging on hippocampal function: plasticity, network dynamics, and cognition. Prog. Neurobiol. 69, 143–179.
Scorcioni, R., Polavaram, S., Ascoli, G.A., 2008. L-Measure: a web-accessible tool for the analysis, comparison and search of digital reconstructions of neuronal morphologies. Nat. Protoc. 3, 866–876.
Seib, D.R.M., Martin-Villalba, A., 2015. Neurogenesis in the normal ageing hippocampus: a mini-review. Gerontology 61, 327–335.
SheikhBahaei, S., Morris, B., Collina, J., Anjum, S., Znati, S., Gamarra, J., Zhang, R., Gourine, A.V., Smith, J.C., 2016. Morphometric analysis of astrocytes in brainstem respiratory regions. J. Comp. Neurol. 526, 2032–2047.
Snyder, J.S., Radik, R., Wojtowicz, J.M., Cameron, H.A., 2009. Anatomical gradients of adult neurogenesis and activity: young neurons in the ventral dentate gyrus are activated by water maze training. Hippocampus 19, 360–370.
Song, H., Stevens, C.F., Gage, F.H., 2002. Astroglia induce neurogenesis from adult neural stem cells. Nature 417, 39–44.
Spampinato, S.F., Bortolotto, V., Canonico, P.L., Sortino, M.A., Grilli, M., 2019. Astrocyte-derived paracrine signals: relevance for neurogenic niche regulation and blood-brain barrier integrity. Front Pharmacol. 10.
Strange, B.A., Witter, M.P., Lein, E.S., Moser, E.I., 2014. Functional organization of the hippocampal longitudinal axis. Nat. Rev. Neurosci. 15, 655–669.
Tanti, A., Belzung, C., 2013. Neurogenesis along the septo-temporal axis of the hippocampus: are depression and the action of antidepressants region-specific? Neuroscience 252, 234–252.
Tavares, G., Martins, M., Correia, J.S., Sardinha, V.M., Guerra-Gomes, S., das Neves, S.P., Marques, F., Sousa, N., Oliveira, J.F., 2017. Employing an open-source tool to assess astrocyte tridimensional structure. Brain Struct. Funct. 222, 1989–1999.
Verkhratsky, A., Augusto-Oliveira, M., Pivoriūnas, A., Popov, A., Brazhe, A., Semyanov, A., 2020. Astroglial asthenia and loss of function, rather than reactivity, contribute to the ageing of the brain. Pflugers Arch. Eur. J. Physiol.
Verkhratsky, A., Ho, M.S., Vardjan, N., Zorec, R., Parpura, V., 2019. General pathophysiology of astroglia. Adv. Exp. Med. Biol. 1175, 149–179.
Verkhratsky, A., Nedergaard, M., 2018. Physiology of astroglia. Physiol. Rev. 98, 239–389.
Verkhratsky, A., Parpura, V., Pekna, M., Pekny, M., Sofroniew, M., 2014. Glia in the pathogenesis of neurodegenerative diseases. Biochem. Soc. Trans. 42, 1291–1301.
Vivar, C., Potter, M.C., van Praag, H., 2013. All about running: synaptic plasticity, growth factors and adult hippocampal neurogenesis. Curr. Top Behav. Neurosci. 15, 189–210.
Wickham, H., 2016. Ggplot2: Elegant Graphics for Data Analysis. Springer-Verlag, New York.
Witter, M.P., Canto, C.B., Couey, J.J., Koganezawa, N., O'Reilly, K.C., 2013. Architecture of spatial circuits in the hippocampal region. Philos. Trans. R. Soc. Lond. B Biol. Sci. 369, 20120515.
2018. Wickham H, François R, Henry L, Müller K. Dplyr: A Grammar of Data Manipulation. https://CRAN.R-project.org/package=dplyr–. (Accessed 6 June 2020).